JOURNAL OF GEOPHYSICAL RESEARCH, VOL. 99, NO. B6, PAGES 12,229–12,243, JUNE 10, 1994

Erosional dynamics, flexural isostasy, and long-lived escarpments: A numerical modeling study

Gregory E. Tucker and Rudy L. Slingerland

Earth System Science Center and Department of Geosciences, Pennsylvania State University, University Park

Abstract. Erosional escarpments are common features of high-elevation rifted continents. Fission track data suggest that these escarpments form by base level lowering and/or marginal uplift during rifting, followed by lateral retreat of an erosion front across tens to hundreds of kilometers. Previous modeling studies have shown that this characteristic pattern of denudation can have a profound impact upon marginal isostatic uplift and the evolution of offshore sedimentary basins. Yet at present there is only a rudimentary understanding of the geomorphic mechanisms capable of driving such prolonged escarpment retreat. In this study we present a nonlinear, two-dimensional landscape evolution model that is used to assess the necessary and sufficient conditions for long-term retreat of a rift-generated escarpment. The model represents topography as a grid of cells, with drainage networks evolving as water flows across the grid in the direction of steepest descent. The model accounts for sediment production by weathering, fluvial sediment transport, bedrock channel erosion, and hillslope sediment transport by diffusive mechanisms and by mass failure. Numerical experiments presented explore the effects of different combinations of erosion processes and of dynamic coupling between denudation and flexural isostatic uplift. Model results suggest that the necessary and sufficient conditions for long-term escarpment retreat are (1) incising bedrock channels in which the erosion rate increases with increasing drainage area, so that the channels steepen and propagate headward; (2) a low rate of sediment production relative to sediment transport efficiency, which promotes relief-generating processes over diffusive ones; (3) high continental elevation, which allows greater freedom for fluvial dissection; and (4) any process, including flexural isostatic uplift, that helps to maintain a drainage divide near an escarpment crest. Flexural isostatic uplift also facilitates escarpment retreat by elevating topography in the vicinity of an eroding escarpment, thereby increasing channel gradients and accelerating erosion which in turn generates additional isostatic uplift. Of all the above conditions, high continental elevation is common to most rift margin escarpments and may ultimately be the most important factor.

Introduction

In the past, most studies of large-scale topography have treated erosion as a secondary modification of what was thought to be a tectonically produced phenomenon. Recent investigations, however, have revealed that the rearrangement of mass at the Earth's surface by weathering and sediment transport also exerts a first-order control on large-scale patterns of tectonic and isostatic uplift [e.g, *Gilchrist and Summerfield,* 1990; *Beaumont et al.,* 1991; *Hoffman and Grotzinger,* 1993]. In this paper, we investigate the role of surface erosion and interactions between erosion and isostasy in generating the asymmetric topography characteristic of many high-elevation rifted margins.

The world's rifted continental margins can be divided into two morphometric types: those with major erosional escarpments and those with relatively subdued relief. Margins with escarpments consist of a band of high local relief separating coastal plains from a low-relief interior plateau. Examples of this type of margin include southern Africa, eastern Australia, western India, eastern Brazil, and eastern Madagascar [*Ollier,* 1985; *Weissel,* 1990]. In some locations, such as the Drakensberg Escarpment in southeastern Africa, the escarpment takes the form of a high, steep, abrupt face of rock [*Ollier and Marker,* 1985]. In others, such as the Namaqualand region of South Africa and Namibia, the escarpment occupies a wide (~70 km) zone of rugged, incised topography that lacks an easily identifiable es-

Paper number 94JB00320.
0148-0227/94/94JB-00320$05.00

carpment face. For purposes of this paper, all these cases will be called a Great Escarpment, defined simply as a belt of high local relief marking the transition from coastal plains to a low-relief interior plateau.

Rift margin escarpments are commonly associated with a marginal topographic upwarp [*Ollier,* 1985; *Weissel and Karner,* 1989]. This association has led to the speculation that these escarpments originate through a combination of base level lowering and marginal uplift during rifting, then subsequently retreat great distances inland across variable lithologies [*Ollier,* 1985; *Partridge and Maud,* 1987]. The long-term persistence of marginal upwarps has been variously explained as residual (nonthermal) rift-related uplift [*Weissel and Karner,* 1989], isostatic uplift in response to denudation [*King,* 1955; *Gilchrist and Summerfield,* 1990; *Stuwe,* 1991], or a combination of the two [*ten Brink and Stern,* 1992]. In any case, the presence of erosional escarpments long after rifting (~150 Ma in the case of southwestern Africa [*Gerrard and Smith,* 1982]) and tens to hundreds of kilometers from the rift hinge zone [e.g., *Gilchrist and Summerfield,* 1990] implies a mode of denudation involving parallel retreat on a grand scale [*King,* 1953, 1955] rather than a more uniformly distributed pattern of denudation [*Davis,* 1899]. That such differential denudation has occurred following rifting in southwestern Africa is supported by fission track data [*Brown et al.,* 1990]. Fission track data from eastern Australia [*Moore et al.,* 1986] and southwest Saudi Arabia [*Bohannon et al.,* 1989] suggest similar patterns.

Previous models of escarpment retreat and isostatic uplift have either assumed a mode and rate of geomorphic development a priori [e.g., *Gilchrist and Summerfield,* 1990; *Stuwe,* 1991] or have been based on simple parameterizations that fail to capture important geomorphic processes such as fluvial erosion. Examples of the latter are models based on linear diffusion, which have been widely used to explore large-scale erosion-geodynamic interactions [e.g., *Moretti and Turcotte,* 1985; *Koons,* 1989; *Flemings and Jordan,* 1989]. In the case of rift margin escarpments, linear diffusion models would predict a gradual relaxation of tectonically produced relief rather than prolonged escarpment retreat. Thus, to explain long-term escarpment retreat on rifted margins, one needs to invoke either inherent nonlinearities in the processes of surface erosion (as suggested by *Weissel* [1990]), external factors such as variable lithology or isostatic uplift, or a combination of these.

In this paper, we use a nonlinear landscape evolution model to define the necessary and sufficient conditions for long-term, long-distance escarpment retreat. We begin by describing the model and presenting a series of simple one-dimensional sensitivity experiments designed to elucidate model behavior. We then apply the model in two dimensions to a high-elevation, escarpment-bounded plateau loosely patterned after the Great Escarpment of southern Africa. Starting with this simple topographic configuration, numerical experiments are presented which explore the role of (1) varying erosion "laws" that represent transport-limited and supply-limited behavior, respectively, and (2) flexural isostatic uplift in response to denudation. These numerical experiments suggest that headward propagation of steep bedrock channels, assisted by (and contributing to) flexural isostatic uplift, provides a viable driving mechanism for prolonged escarpment retreat.

Landscape Evolution Model

Conceptual Overview

The landscape evolution model used in this study represents topography as a grid of cells with varying elevations (Figure 1a). Cell elevations evolve according to computed fluxes of material among cells. As in the model of *Ahnert* [1976], the model landscape is composed of two basic materials: "rock", which represents consolidated or jointed but otherwise unweathered bedrock, and "sediment", which represents stream sediment, colluvial deposits, and weathered residuum. Rock may be subdivided into different strata with varying resistance to weathering, erosion, and slope failure. Model equations are listed in Table 1. The model maintains continuity of rock and sediment (equations (T1), (T2), and (T3)), plus continuity of water (equation (T4)).

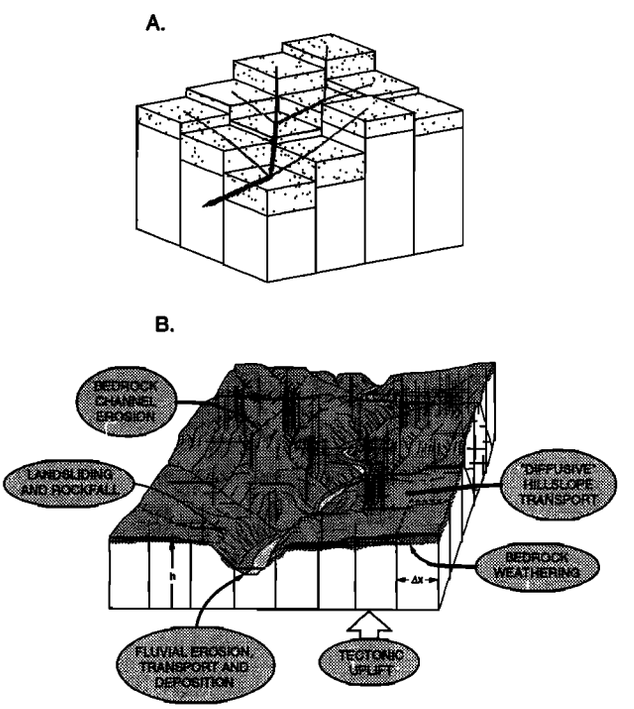

Figure 1. Conceptual illustration of the landscape evolution model. (a) Model representation of topography and drainage. Each cell is Δx by Δx in its horizontal dimensions and consists of one or more lithologies capped by a variably thick sediment cover (stippled). Streams flow in the direction of the steepest slope. (b) Illustration of processes incorporated in the model. Adapted from *Strahler* [1978].

Table 1. Processes represented in the landscape evolution model

Process	Governing Equation	Table Equation
Continuity of rock	$\partial R/\partial t = U(x,y,t) - [E_W + E_{MF} + E_{BR}]$	(T1)
Continuity of sediment	$\partial C/\partial t = E_W + E_{MF} + E_{BR} - \nabla(q_s + q_{LS} + q_D)$	(T2)
Elevation changes	$\partial h/\partial t = \partial R/\partial t + \partial C/\partial t$	(T3)
Continuity of water	$Q = AP$	(T4)
Drainage routing	steepest descent algorithm (see text)	-
Bedrock weathering	$E_W = k_w \exp(-m_w C)$	(T5)
Fluvial sediment transport	$q_s = k_f q S$	(T6)
Lowering rate of a cell due to bedrock channel incision	$E_{BR} = (k_b/\Delta x) Q S$	(T7)
Shallow landsliding (q_{LS})	oversteepened sediment masses instantaneously collapse	-
Rock mass failure (E_{MF})	oversteepened rock masses instantaneously collapse	-
Diffusive hillslope transport	$q_D = -k_d \nabla h$ (flux cannot exceed available sediment)	(T8)
Lithosphere flexure	$D(d^4w/dx^4) + (\rho_m - \rho_s)gw = l(x)$	(T9)

The landscape evolution model accounts for the following processes (Figure 1b and Table 1): the routing of surface water into drainage networks, weathering of bedrock to create a moveable sediment cover, sediment transport by streams, stream incision into bedrock, slope failure, diffusive hillslope transport, and flexural isostatic uplift in response to denudation. While this list does not capture all the processes known to geomorphologists, we think it is the minimum that should be considered. The following sections describe how each process is modeled.

Drainage Networks

The present model addresses landscape evolution on a regional scale, with cells of the order of 1 km^2 or more. Thus model cells conceptually contain both channel and hillslope elements, with multiple low-order channels or hollows in addition to an explicitly modeled major channel. Hillslope processes are conceived to occur on both the macroscale and on the subgrid scale. In the latter case, it is assumed that sediment delivery from hillslopes to channels occurs on a short timescale relative to the timescale for channel erosion, so that all of the sediment within any given cell is available for transport by the fluvial system. This assumption is justified by noting that in high-relief areas hillslope transport is likely to be dominated by landsliding, a process which tends to maintain slopes near a materially dependent equilibrium value and thus promotes a short response time.

During each time step, water flows from each cell in the direction of steepest slope toward one of eight surrounding cells (Figure 1a). The discharge at any point on the grid is then computed as the integral of precipitation over all cells that drain to that point. If uniform precipitation is assumed, this implies that discharge is linearly proportional to drainage area (equation (T4)). The precipitation value used for these models represents an "effective" precipitation, analogous to the effective or dominant discharge concept [*Wolman and Miller,* 1960], rather than a mean annual value.

Sediment Production

This model differs from several proposed recently [*Willgoose et al.,* 1991; *Chase,* 1992; *Beaumont et al.,* 1992] by explicitly addressing the role of sediment production. The term "weathering" is used herein to refer to the instantaneous production of moveable, uniformly-sized sediment from solid bedrock, after the manner of *Ahnert* [1976] and *Anderson and Humphrey* [1990]. While variable grain size could be taken into account, such a treatment greatly complicates the numerical solution to the governing equations. At present, grain size is assumed to be constant.

It is commonly understood that low sediment production rates strongly influence the rate and style of landform erosion in arid regions [e.g.,*Anderson and Humphrey,* 1990]. This may also be the case in steep, humid landscapes where sediment transport rates equal or exceed production rates [e.g.,*Iida and Okunishi,* 1983]. We assume that sediment production rates decay exponentially as the sediment mantle becomes thicker. We therefore follow *Ahnert* [1976] and *Anderson and Humphrey* [1990] in adopting equation (T5) (Table 1)

to describe the rate of descent of a weathering front. Note that isovolumetric weathering is assumed, implying that the change in density upon conversion of rock to sediment is compensated for by removal of mass in solution. The same assumption is made for the two other sediment-generating processes in this model, bedrock channel erosion and rock mass failure.

Alluvial and Bedrock Channels

Central to the model's treatment of fluvial processes is the distinction made between bedrock and alluvial channels. Recent studies [*Howard and Kerby,* 1983; *Seidl and Dietrich,* 1992] confirm the view of *Gilbert* [1877] that these two channel types represent very different physical processes. Bedrock channels have been defined as those "which lack a coherent bed of active alluvium" [*Howard,* 1987]. It has been suggested that the erosion of bedrock channels may be described as a simple function of slope and drainage area:

$$\frac{\partial h}{\partial t} \propto A^{\alpha} S^{\beta} \tag{1}$$

where h is channel bed elevation, t is time, A is drainage area, S is channel bed slope, and α and β are constants [*Howard et al.,* 1992, this issue]. If discharge is linearly proportional to drainage area, this becomes

$$\frac{\partial h}{\partial t} \propto Q^{\alpha} S^{\beta} \tag{2}$$

where Q is an effective or dominant discharge [*Wolman and Miller,* 1960]. Analysis of slope/area ratios at bedrock channel tributary junctions in the Oregon coast ranges [*Seidl and Dietrich,* 1992] suggests a stream power dependent erosion law, with exponents $\alpha = \beta = 1$. This equation forms the basis for the treatment of bedrock channel erosion in the model (equation (T7), Table 1). The details of its implementation on a planform grid are described below.

Most of the equations for sediment entrainment and transport in alluvial channels [*Yalin,* 1977] can be simplified to the general form

$$q_s \propto q^m S^n \tag{3}$$

where q_s is volumetric sediment transport rate per unit channel width, q is discharge per unit channel width, and m and n are constants [*Howard,* 1980]. If channel width is assumed to vary systematically with discharge as $W \propto Q^p$ [*Leopold et al.,* 1964], this becomes

$$Q_s = k_f Q^{(p+m-mp)} S^n = k_f Q^{m_f} S^{n_f} \tag{4}$$

where Q_s is volumetric sediment flux, k_f is a constant, and m_f incorporates both m and p. The exact values of these exponents are not critical parameters for the purposes of this study. Values for m_f and n_f vary around 1; in this study, they are both set equal to 1, thereby approximating the *Bagnold* [1966] bed load equation.

Because transitions between channel types in nature appear to be abrupt [*Howard,* 1980], the bedrock-alluvial transition is here modeled as a threshold phenomenon. During each time step, a pass is made from the highest through the lowest cells. For each cell, potential fluvial erosion or deposition is calculated according to a simple continuity of mass equation:

$$\frac{\Delta h}{\Delta t} = \frac{Q_s{}^{(in)} - Q_s{}^{(out)}}{\Delta x^2} \tag{5}$$

where Δh describes the change in a cell's elevation over a time interval Δt and Δx^2 is the surface area of the cell. If the net sediment flux out of a cell is less than the total sediment available, the cell elevation is adjusted and the outward sediment flux is delivered to the adjacent downstream cell (Figure 2a). If the net potential sedi-

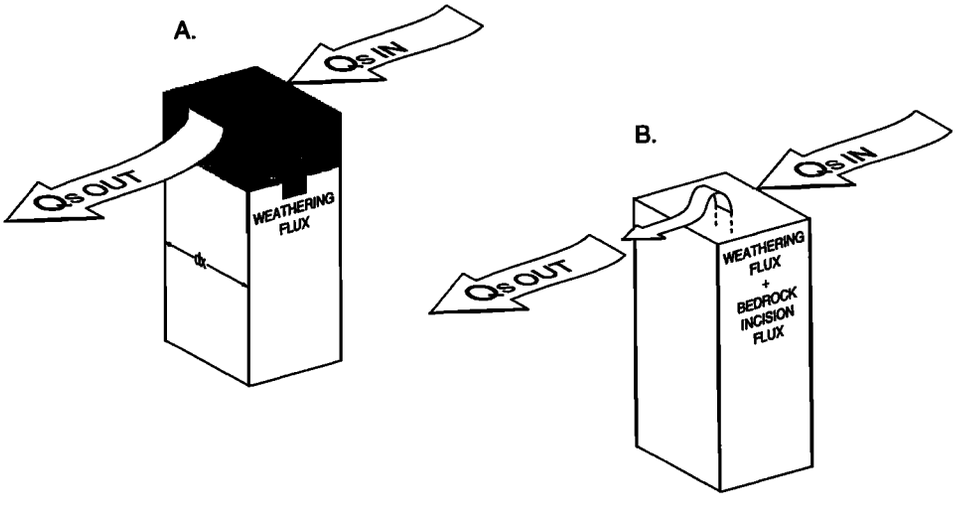

Figure 2. Sediment fluxes in model cell with horizontal dimension Δx and sediment cover thickness C. (a) Transport-limited case: the rate of change in elevation is equal to the sediment flux in minus the flux out, divided by the area of the cell. (b) Supply-limited case: the rate of change in elevation is equal to the bedrock weathering rate plus the flux due to bedrock channel erosion.

ment flux from a cell is greater than the total sediment available (Figure 2b), the cell is flagged as containing a bedrock channel and the outflux is set equal to the total sediment in the cell at the start of the time step plus the flux due to bedrock channel erosion (equation (T7), Table 1). The operational definition of a bedrock channel therefore is one in which the fluvial carrying capacity (integrated over a time step) is greater than the total sediment supply, which consists of both sediment delivered from upstream and sediment produced and/or previously deposited within a cell. Where the amount of excess carrying capacity is less than the potential sediment flux due to channel erosion, channel erosion is limited to that amount which just satisfies the fluvial carrying capacity.

Some consideration needs to be given to the way in which equation (2) is applied across an entire cell, in as much as it describes the erosion rate in a channel irrespective of surrounding hillslopes. Unless channels and hillslopes are modeled separately [*Howard et al.*, 1992, this issue; *Anderson*, this issue], there are two obvious approaches. The first is to assume that hillslopes are perpetually in equilibrium with the rate of channel lowering, so that an entire cell will lower at the same rate as its principle channel. While this approach might be valid for near-steady-state topography, in other cases it fails to capture important time lags between channel bed erosion and hillslope response. For the type of problem considered in this study, this approach would tend to overpredict denudation rates, with the degree of overprediction being dependent upon grid cell size. A second approach, and the one employed in this study, is to view channel incision in terms of mass flux. Consider a square region of dimensions Δx by Δx containing a single major channel. The average lowering rate across that region due to channel incision is

$$\frac{\partial h}{\partial t} = -\frac{1}{\Delta x^2} \int_0^L W(l)\, E(l)\, dl \tag{6}$$

where l is distance downstream, L is the total length of the channel within the region of interest, W is channel width, and E is the channel bed erosion rate. Substituting equation (2) for E and assuming constant W, Q, and S along the reach, equation (6) becomes

$$\frac{\partial h}{\partial t} = -\frac{LW}{\Delta x^2} k Q^{\alpha} S^{\beta} \tag{7}$$

where k is a proportionality constant. If channel length is proportional to Δx and assuming $a = b = 1$, the average lowering rate of a cell due to channel erosion is proportional to local stream power, scaled by the width of the cell (equation (T7), Table 1):

$$\frac{\partial h}{\partial t} = -\frac{k_b}{\Delta x} QS \tag{8}$$

Hillslope Processes

The model recognizes two types of hillslope process: slow, continuous mass movement, and mass failure. Slow hillslope processes include soil creep, rain splash, and bioturbation. We model these as diffusion processes (equation (T8), Table 1), modified so that sediment flux does not exceed sediment supply [*Anderson and Humphrey*, 1990]. Thus, if sediment thickness is zero, the diffusive sediment flux is also zero even though slopes may be large. Diffusive sediment transport is considered in only one of the model experiments presented below.

The basic idea behind the model's treatment of mass failure is that any slopes that become steeper than a specified threshold angle will fail, initiating a "landslide" that cascades downhill until a stable slope angle is reestablished. During the course of a time step, this slope failure algorithm is repeated until no oversteepened slopes remain, ensuring that cases of multiple oversteepened cells and cases in which one collapse triggers others are handled correctly. In so far as the material strength of rock masses is typically much greater than that of unconsolidated hillslope debris [*Carson and Kirkby*, 1972], separate slope failure angles may be defined for sediment and for bedrock. So we are really modeling two types of mass failure: shallow debris landsliding and rock mass failure. The same basic algorithm is used to compute both types of mass failure, with two differences: (1) "sediment slides" are limited by material availability (i.e., a slide can only happen if sediment is present), and (2) in the case of bedrock mass failure, "slope" is considered to be the average slope from the bedrock-sediment contact in one cell to the surface of an adjacent cell. The behavior of this slope failure algorithm is illustrated in the model examples described below (Figures 6b-6d).

Treatment of Drainage Divides

Modeling fluvial erosion in drainage networks is a moving boundary problem in which the moving boundaries are drainage divides. At a drainage divide, drainage area and thus discharge are zero by definition, so that by equation (T7) (Table 1) channel erosion will also be zero at a divide. As discussed above however, cells in the model conceptually contain both channel and hillslope elements, and drainage divides are really subgrid scale features. We deal with this by tracking both a mean elevation and a peak elevation for divide cells. The difference between these is that the peak elevation is not subject to bedrock channel erosion. (This is similar but not identical to the "pinned divide" technique of *Kooi and Beaumont*, [this volume]). The peak elevation is used for all computations, including computation of flow routing. The mean elevation is plotted. For purposes of this study, a "divide cell" is one which forms a surface convexity in either principle grid direction. Divide cells therefore include saddles as well as peaks and ridges. Alternatively, divide cells could be defined as those which receive flow only via precipitation. This method produces similar results, but the algorithm is more complicated. Other processes, including fluvial sediment transport, are allowed at divide cells. For any cell whose channel is fed only by precipitation, the mass

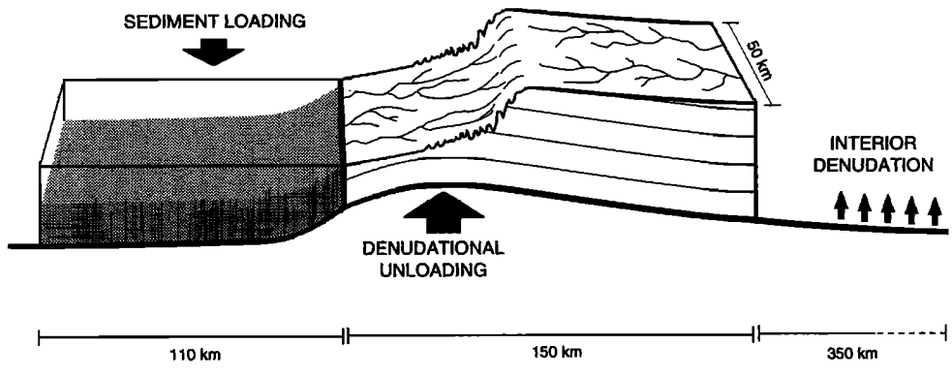

Figure 3. Illustration of the coupled denudation-flexural isostasy model, showing the distribution of isostatic loading and unloading. The model domain is 150 km by 50 km. Surface loads are applied to the one-dimensional flexure model by averaging in the direction parallel to the fixed coastal boundary. Sediment delivered to the coastal boundary is uniformly distributed across a 110-km-wide shelf.

flux out due to fluvial sediment transport (as long as sufficient sediment is available) is therefore

$$Q_s = \frac{k_f Q S}{\Delta x^2} = k_f P S \qquad (9)$$

where P is the precipitation rate (dimensions of L/T).

Flexural Isostasy

As denudation progresses, elevations in the model grid can respond according to the equation for deflection of an elastic beam overlying an inviscid fluid (equation (T9), Table 1) [*Turcotte and Schubert*, 1982]. No horizontal forces are considered. Because this study addresses cases in which denudation tends to vary strongly only in one direction (perpendicular to the strike of an eroding escarpment), a one-dimensional flexure model is used. Loads are calculated by averaging in a direction parallel to the fixed model boundary. Although flexural rigidity typically varies across passive margins [e.g., *ten Brink and Stern*, 1992], for the sake of simplicity it is treated as spatially constant here. The effect of this assumption will generally be to underpredict the degree of flexure near the margin relative to that in the interior.

For the passive margin experiments presented below, offshore sediment loads are calculated by summing the total sediment load reaching the coastal boundary. This load is uniformly distributed across a shelf 110 km wide [*Bremner et al.*, 1988]. Because natural flexural wavelengths are typically larger than the 150-km region in which surface processes are modeled in these experiments, the flexure model extends an additional 350 km beyond the surface model grid (Figure 3). For purposes of flexural calculation, the denudation rate beyond the landward erosion model boundary is assumed to be equal to the average denudation rate near that boundary.

Numerical Implementation

During each time step, drainage directions are recomputed, and a pass over the grid is made from the highest to lowest cells. To improve accuracy and stability, computation of fluvial sediment transport and bedrock incision is broken up into one or more sub-time steps using a recursive algorithm, with the size of the smaller steps based on an estimated maximum stable time step size. Sediment production during each time step is computed using an analytical solution to equation (T5) (Table 1), which is considerably more accurate and stable than a simple finite difference approximation. Diffusive hillslope transport is computed using a forward extrapolation finite difference method. The model has been extensively tested for convergence and robustness and is virtually insensitive to time step size as long as time steps are sufficiently small relative to the process rate coefficients.

Model Results: One-Dimensional Models

Starting from the premise that rifting creates a topographic asymmetry, our aim is to identify the necessary and sufficient conditions for the preservation of this initial asymmetry. Clearly, one requirement must be that the processes which undercut and steepen an escarpment are more efficient than those which dampen and diffuse it. A simple static model (Figures 4a-4c) illustrates the tendency of diffusive models based on the continuity equation to dampen relief. The bedrock erosion model (equation (T7), Table 1, and Figure 4d), by contrast, predicts not only perpetuation but also steepening of slope discontinuities through time. While such behavior may be unrealistic at the scale of small knickpoints [e.g., *Gardner*, 1983], there is no a priori reason to reject this model at larger scales. The nature of equation (T7) (Table 1) already suggests that lateral migration of relief may be a common behavior in supply-limited fluvial systems dominated by bedrock channel incision.

We begin by considering the simplest case in which the effects of flow convergence and divergence are ignored, so that the problem may be reduced to one

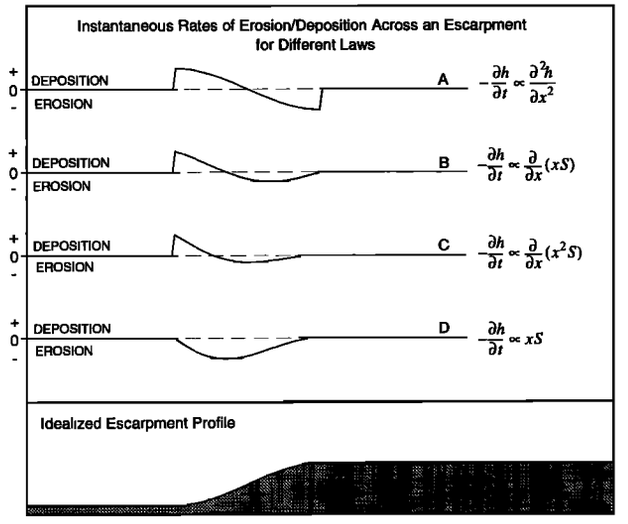

Figure 4. Static model showing instantaneous rate of erosion/deposition across an idealized escarpment (bottom) for various erosion laws. (a) Erosion/deposition rates for diffusion equation. (b) Erosion/deposition rates for stream power transport law, assuming discharge Q proportional to distance from divide x. (c) Erosion/deposition rates for stream power transport law, assuming discharge proportional to x^2. (d) Erosion rates for stream power erosion law, assuming Q proportional to x.

dimension. An idealized representation of a high-elevation rifted continent (profile $t = 0$ in Figure 5a) is used as an initial condition. This initial topography consists of a plateau that gently slopes to the east (1 m/km, or ~0.06°) and terminates in a steep slope (600 m/km, or ~31°) at the western edge. The western boundary at $x = 0$, representing a nonprograding shoreline, remains fixed throughout each simulation. The eastern (interior) boundary at $x = 150$ km is continually adjusted to maintain a finite slope, equal to the slope immediately adjacent to that boundary. The plateau's maximum elevation is 1200 m, based on an estimate of the prerift elevation of southwestern Africa [*Gilchrist and Summerfield,* 1990].

The position of the initial drainage divide at the escarpment crest is based on the assumption that rift flank uplift early in a margin's evolution would divert drainage inland away from the margin [*Summerfield,* 1991], as is the case today, for example, in the northwestern Red Sea region. Modern drainage divides lie at or near the crest of the Western Ghats escarpment in India, most of the Great Escarpment of southern Africa, and parts of the eastern Australian escarpment (as discussed below). In the absence of significant post rift margin uplift, we find it highly unlikely that these divides could have migrated seaward after the cessation of rift-related uplift. Thus it is reasonable to assume that in most of these cases the principal drainage divide at the time of rifting was not located very far inland. However, the effects of rapid divide migration following base level drop will be explored below.

Transport-Limited Models

When escarpment erosion is modeled by a simple diffusion equation (Figure 5a), the initial relief is smoothed out, and denudation is distributed over a wide area. Lateral retreat does not occur. When sediment transport across an escarpment is modeled as a function of local stream power (Figure 5b), with discharge proportional to distance from the drainage divide so that

$$-\frac{\partial h}{\partial t} \propto \frac{\partial q_s}{\partial x} \propto \frac{\partial xS}{\partial x} = x\frac{\partial^2 h}{\partial^2 x} + \frac{\partial h}{\partial x} \qquad (10)$$

then the dependence on distance from the drainage divide leads to amplified erosion and deposition away from the divide (Figure 4b). Nonetheless, the process retains a strong diffusive component (first term in equation

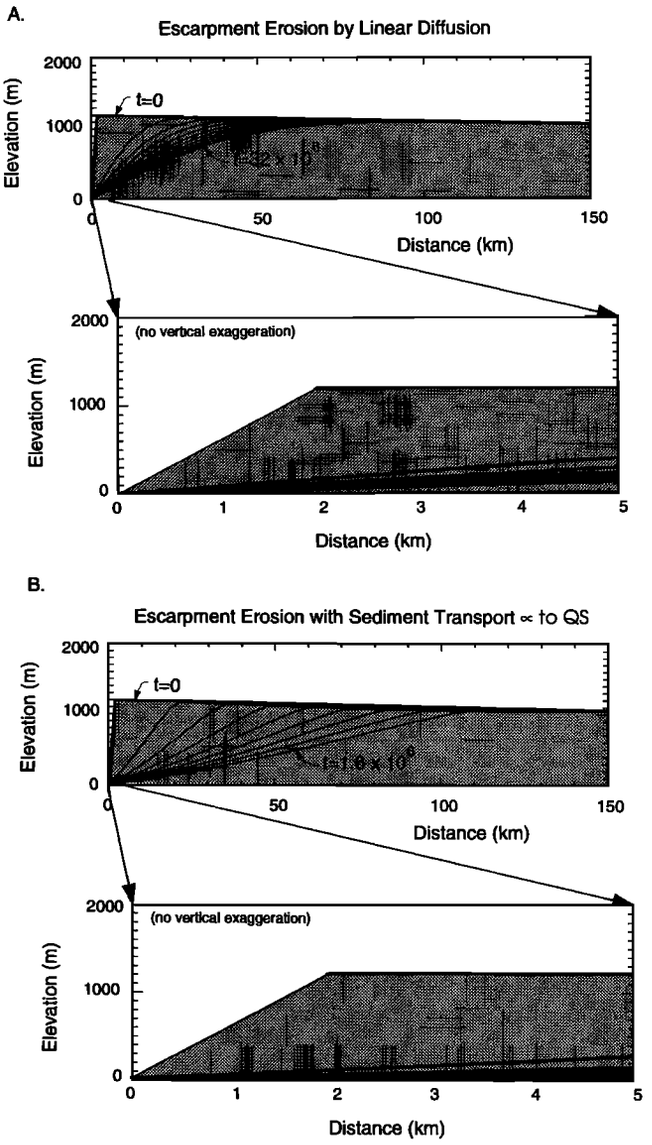

Figure 5. Evolution of initial escarpment profile (a) by linear diffusion and (b) by a stream power-dependent transport law. Model domain consists of 750 nodes with $\Delta x = 200$ m. The insets show an enlargement of the left most 5 km for comparison with Figures 8 and 9.

(10)) which tends to dissipate sharp concavities (and convexities, except near the drainage divide). Divide migration in this example results from differential denudation on either side of the divide. One of the crucial assumptions here is that in the transport-limited case, removal of mass by channelized flow is the limiting factor for divide migration. If this were not the case (if, for example, hillslope transport above channel heads were highly inefficient relative to first-order channels) then the slopes above channel heads would steepen until a new equilibrium was established. Thus treating fluvial transport as the limiting factor for divide migration in the transport-limited case is equivalent to assuming that equilibrium is always maintained at the hillslope scale. This assumption is reasonable as long as the time scale for adjustment is short relative to overall denudation rates.

Supply-Limited Models

Supply-limited models based on weathering-limited diffusive hillslope transport have been explored by *Anderson and Humphrey* [1990]. Here, we begin by examining the extreme case in which weathering rates are zero, so that sediment production and removal occurs only through fluvial channel erosion (Figure 6). Since $Q = A = 0$ at drainage divides, channel erosion alone is incapable of moving a divide. Thus, in the first example (Figure 6a) the drainage divide remains fixed. Immediately downstream from the divide, the profile steepens as a result of increasing stream power. Near the fixed boundary, the bed slope is reduced to the point at which it becomes just sufficient to transport the total sediment flux and no more. As the upper portion of the profile continues to steepen, this lower graded reach propagates upstream. The graded reach is technically a bedrock channel, because it is actively eroding. However, the erosion rate in this case is limited by the channel carrying capacity. The transition from ungraded to graded reach coincides with a concave break in slope. Similar slope breaks that appear to coincide with a change in process have been observed in the field [e.g.,*Howard and Kerby,* 1983; *Seidl and Dietrich,* 1992], although the cause and effect relationships in these instances are not clear.

In the absence of other processes, the upper profile in this simple model will continue to steepen until a vertical face is created at the drainage divide. In reality, we would expect that some form of mass flow or failure would be activated as the channel gradients increase. Here, we model this effect by simply assuming that slopes above a threshold gradient will collapse, shedding mass downslope until the threshold gradient is reestablished. When this type of rule is imposed (Figures 6b-6d), parallel retreat commences as soon as the channel profile reaches the threshold gradient. The retreat rate is governed by the maximum channel erosion rate, which occurs near the slope break. Since the rate of lowering at this point is in part a function of slope length (distance from the divide), it turns out that the retreat rate is inversely proportional to the threshold gradient.

This simple model of channel profile evolution has much in common with the conceptual slope models of *Penck* [1953]. If the tendency for bedrock channels to steepen through time is real, then such steepening

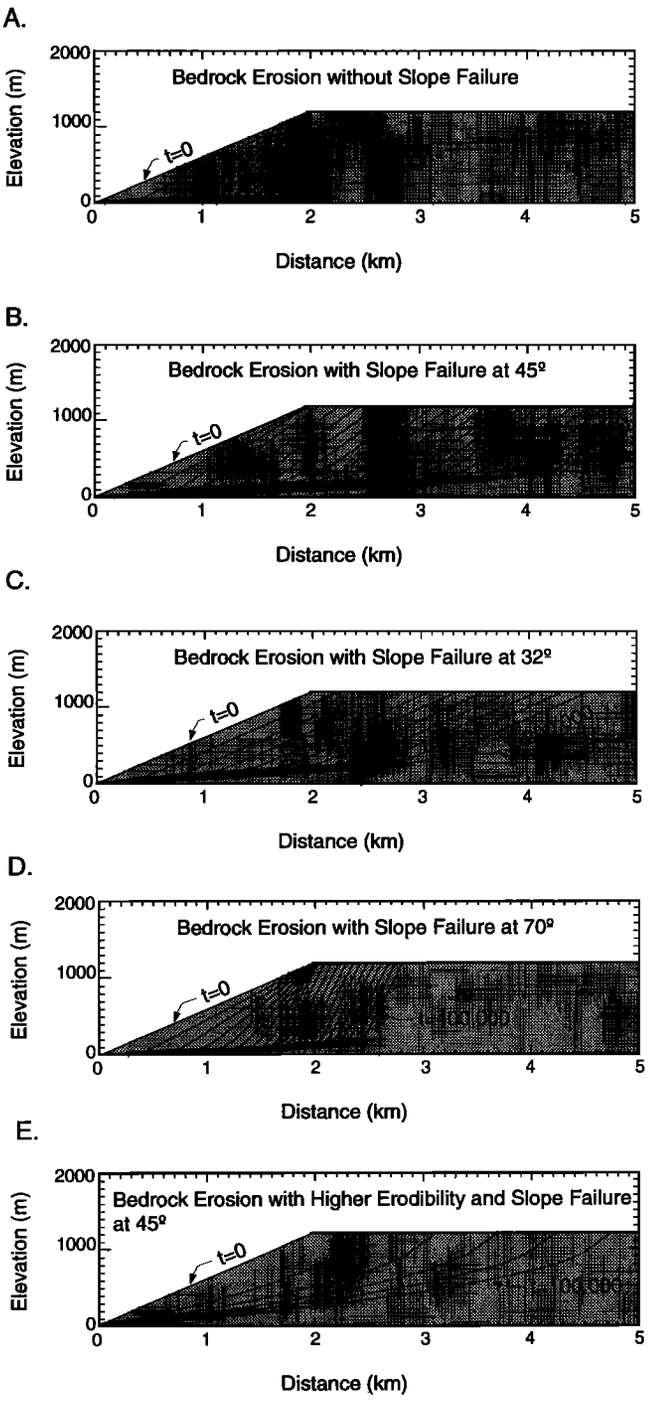

Figure 6. Evolution of escarpment profiles by bedrock channel erosion. Sediment production by weathering is zero for each run. Model domain consists of 250 nodes with $\Delta x = 20$ m. In each simulation except Figure 6e, $k_f = 0.1$ (dimensionless) and $k_b = 10^{-5}$ m^{-1}. (a) Bedrock channel erosion only. (b) Bedrock channel erosion, with slope failure at 45°. (c) Bedrock channel erosion, with slope failure at 32°. (d) Bedrock channel erosion, with slope failure at 70°. (e) $k_b = 10^{-4}$ m^{-1}, slope failure at 45°.

should ultimately trigger slope failure, resulting in parallel retreat. We have not considered the role of debris flows, which in many instances may become important agents of channel erosion at high gradients [e.g., *Seidl and Dietrich*, 1992]. However, the effect of debris flows, which require a finite drainage area, should be similar to that of other bed erosion processes: steepening headwater slopes to the point of collapse. Thus this model suggests that when hillslope sediment production rates are low, drainage divide migration will be driven by a form of parallel retreat involving channel downcutting and slope failure.

There is an interesting feedback relationship between the efficiency of fluvial transport (parameter k_f) and that of bedrock channel erosion (parameter k_b). The ratio k_f/k_b governs the distance over which a channel segment reaches its carrying capacity (in this sense the ratio k_f/k_b is somewhat analogous to the "erosion length scale" of *Beaumont et al.* [1992]). When k_f/k_b is decreased, the channel comes to capacity over a shorter distance (Figure 6e). The result is an increase in the length of the graded reach, as well as an increase in the graded slope required to transport material derived from bed erosion upstream. This relationship is important because the total relief on the steep ungraded reach is limited by the need to maintain a certain minimum slope out to base level. From this finding emerges a simple generalization: the more efficiently the fluvial system transports sediment, the lower the slope required to carry sediment from an active erosional front out to base level (the coastline in these examples). A lower transport slope allows for greater relief along the active erosion front.

Low Weathering Rate Models

So far two extreme cases have been considered: the transport-limited case, and the case in which sediment production occurs only through bedrock incision or mass failure. We now consider the case in which sediment is supplied to the channel by both channel incision (equation (T7) (Table 1)) and weathering (equation (T5) (Table 1)). The pattern of profile development in this case is intermediate between the end-member cases discussed previously (Figures 7a and 7b). The biggest impact of introducing a finite weathering rate is upon drainage divide migration. Recall that our rule for drainage divides specifies that sediment may be transported out of divide cells but that bedrock channel incision is not allowed. Thus the introduction of weathering means that divides may now migrate by differential sediment transport, provided that the total sediment transport out of a divide cell does not exceed the bedrock weathering rate. This results in a rapid rate of divide migration landward relative to the retreat rate of the steep portion of the alluvial profile (Figure 7a). A curious feature of these models is that any weathering rate, as long as it is large enough to exceed transport rates on the low-gradient interior, will produce rapid divide migration. This seems to be an artifact of the assumption that fluvial channel transport is the limiting factor for divide migration. Because our goal is

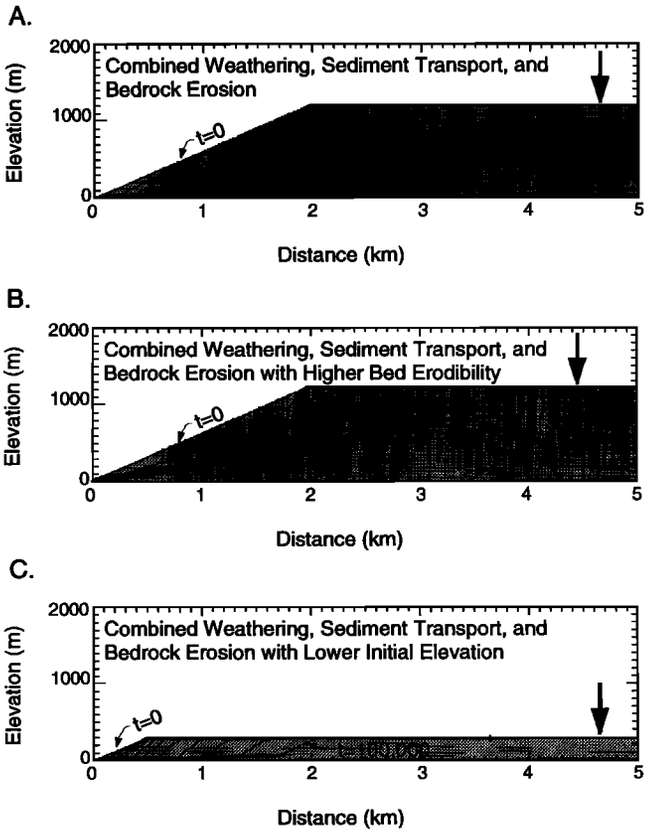

Figure 7. Evolution of escarpment profiles by weathering, sediment transport, and bedrock channel erosion. Model domain is the same as in the runs of Figure 6. For each simulation, the bedrock sediment production rate k_w equals 5 x 10^{-5} m/yr and the fluvial transport efficiency parameter, k_f, equals 0.1. (a) $k_b = 10^{-5}$ m^{-1}. (b) $k_b = 10^{-4}$ m^{-1}. (c) Same as Figure 7a but with lower initial elevation. The large arrows show the position of the drainage divide at the time of the last profile.

to model landscape erosion on regional scales, we have not attempted to incorporate processes and properties appropriate to the scale of drainage divides. It may be, however, that drainage divide migration in the low-gradient uplands above an escarpment depends strongly on short-range hillslope processes, erosion thresholds, and hillslope hydrology, none of which are easily modeled at a grid resolution of 1 km^2 or more.

When the rate of drainage divide advancement is greater than that of the steep channel profile, the steep reach essentially becomes a kilometer-scale knickpoint (Figure 7). The behavior of knickpoints for a stream power-dependent erosion law has been explored by *Howard et al.* [1992, this issue]. The added complexity in this situation is that channel discharge increases as the knickpoint propagates upstream. In this model, its behavior will depend critically upon the balance between fluvial transport efficiency (parameter k_f) and bed erosion efficiency (parameter k_b). Where transport is relatively efficient (Figure 7a), the steep reach will continue to steepen, ultimately perhaps to the point of triggering other processes. Where bed erosion is relatively efficient (Figure 7b), the increased sediment flux

from upstream will cause the graded reach to overtake the knickpoint, decreasing its gradient and eventually eliminating it. This same behavior ought to be generally true for any process which increases the sediment flux in the channel.

The tendency of bedrock channel profiles in these models to steepen and propagate laterally through time suggests a basic mechanism for long-term escarpment retreat. Parallel retreat of a steep channel profile will occur if that profile steepens to the point at which some threshold-dependent, slope-driven process is activated. In this case, we would expect to find drainage divides near the head of steep channel reaches. Alternatively, lateral retreat of a steep channel profile can still occur according to this model if drainage divides in the uplands migrate faster than the steep channel reach. In this case, steep channel reaches essentially behave as kilometer-scale knickpoints. In either scenario, the ratio of sediment production to sediment transport capacity emerges as an important variable. At some point downstream, the sediment feed rate will become large enough and the gradient low enough that the channel will approach its transport capacity and the rate of bed erosion will be reduced. Where capacity is large relative to the feed rate, the slope on this graded reach will be low, thus allowing for greater relief between the uplands and the base of the ungraded reach. Although we have focused on transport capacity rather than competence, grain size characteristics clearly influence the shape of graded river profiles [*Snow and Slingerland,* 1987]. Were these models to account for a downstream increase in competence (due to decreasing particle size and increasing flow energy), the effect would be to produce a more concave profile and thereby amplify the tendency for headwater steepening and parallel retreat.

So far, we have discussed some possible controls on lateral retreat of river channel profiles. In the following section, we explore the conditions under which the migration of channel profiles might produce escarpment retreat, in the sense of lateral progression of a coherent band of high local relief. First, it is worth noting that the tendency for prolonged migration of a steep channel profile is also a function of initial relief. Where, for example, the initial plateau is lower, profile steepening is inhibited (Figure 7c). This suggests that high initial relief is an important factor in determining whether prolonged retreat will occur.

Model Results: Two-Dimensional Models

A migrating channel profile is not necessarily the same as a retreating escarpment. One might imagine, for example, that headward channel advance would create a dissected plateau rather than a retreating escarpment. In this section, we use the full two-dimensional model to explore the effects of drainage convergence and branching. An additional experiment investigates the coupling between denudation and flexural isostatic uplift.

For each of these experiments, a 150 by 50 cell grid with 1 km^2 cells is used to represent a 1200-m-high plateau bounded on one side by a steep slope (0.3 m/m, or ~17°) (Figure 8a). This slope is equal to the threshold failure angle defined below, since anything steeper than this would simply collapse during the first time step. The plateau slopes gently downward (10^{-3} m/m, or ~0.06°) away from the crest at the slope break, just as in the one-dimensional (1-D) experiments. This initial surface is roughened by adding a small amount of fractally-distributed random noise having a standard deviation of ~3.8 m. The west (left-hand) boundary is held fixed throughout the simulation, while the east (right-hand) boundary is adjusted to preserve the average slope immediately adjacent to that boundary. The north and south (top and bottom) boundaries are joined together to minimize edge effects. This is done by treating cells along the north edge of the grid as if they were adjacent to those along the south edge, and vice versa. Any flow reaching the north or south boundary is then rerouted to its equivalent position on the opposite edge of the grid.

Transport-Limited Versus Supply-Limited Models

Just as in the 1-D case, the balance between sediment supply and transport capacity has a profound impact on model landscape properties in the 2-D case (Figures 8b and 8c). In the transport-limited experiment (Figure 8b), the initial substrate consists entirely of sediment, just as in the one-dimensional experiment of Figure 5b. In the supply-limited experiment of Figure 8c, the initial substrate consists of bedrock, with the bedrock weathering rate (parameter k_w) set to a finite but small value (5×10^{-5} m/yr). For these experiments, the threshold slope for failure (both rock and sediment) is set at 0.3 m/m. A low value is used here because the model cannot resolve slopes on a scale smaller than $\Delta x = 1000$ m. In the supply-limited case, the high local relief results from strong differential incision between large and small drainages. This differential incision occurs because of the strong dependence of erosion rate upon drainage area in the bedrock erosion equation (T7) (Table 1). Recall that for capacity-limited alluvial channels, equation (T6) (Table 1) dictates that the erosion rate is a function of the spatial gradient in drainage area rather than its absolute value. Thus one of the predictions of the bedrock erosion model is that bedrock channels should generate much greater local relief than, for example, alluvial channels downcutting through noncohesive sediment. The predicted differences would diminish for larger exponents on the alluvial sediment transport law (equation (T6) (Table 1)) or smaller exponents on the bedrock channel erosion law (equation (T7) (Table 1)). We have presented only the end-member cases here.

A second notable feature of the supply-limited experiment (Figure 8c) is the presence of a series of large valleys propagating headward into the interior. There is no escarpment here, at least in the sense of a laterally

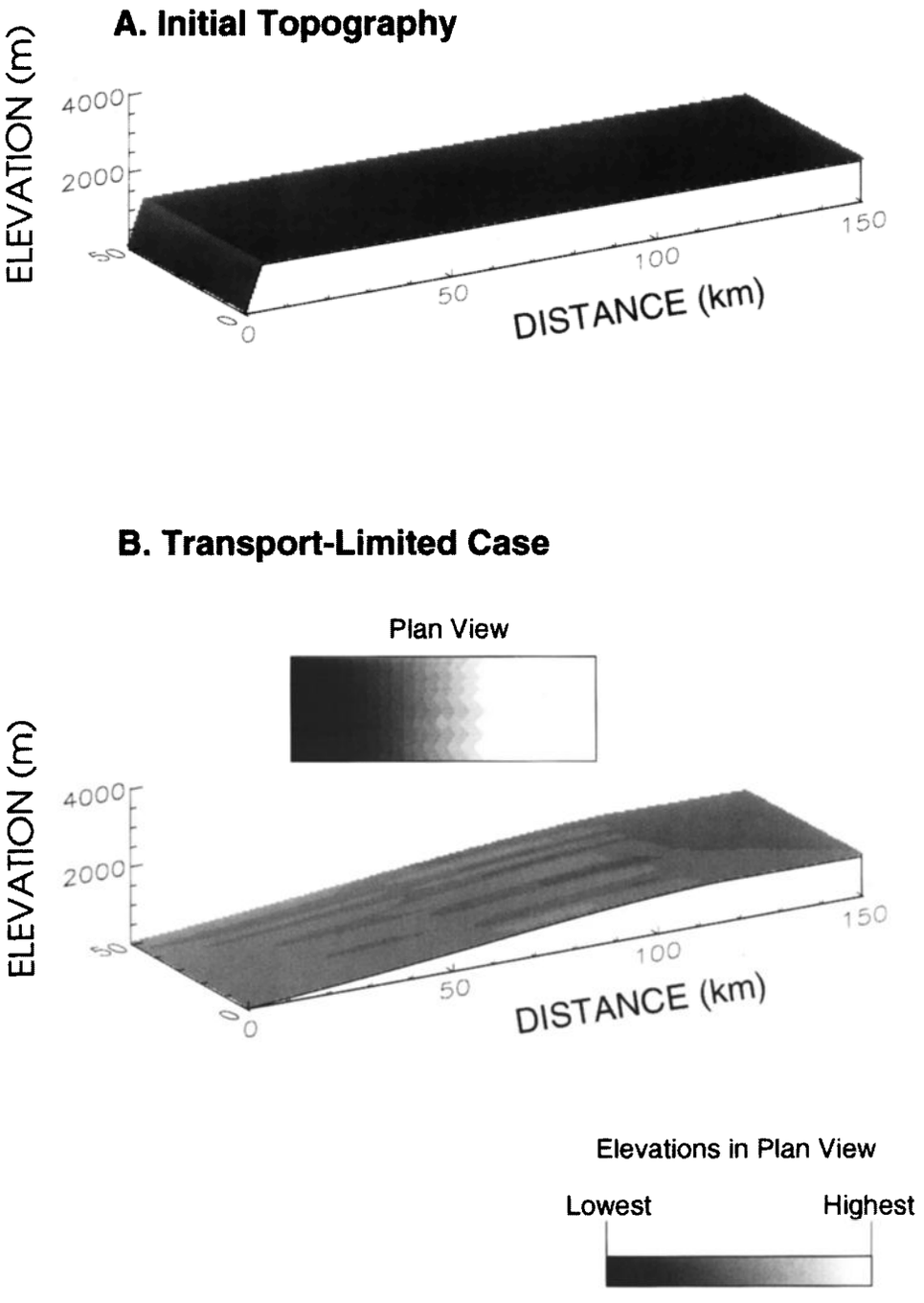

Figure 8. Two-dimensional models of escarpment erosion. Grid size is 150 by 50 with 1 km^2 cells. For each simulation $k_f = 0.1$. For the simulations shown in Figures 8c and 8d, $k_b = 10^{-5}$ m^{-1} and $k_w = 5 \times 10^{-5}$ m/yr. Critical failure angle in each is 0.3 m/m, or ~17°. (a) Initial topography. (b) Simulation with initial substrate consisting of cohesionless sediment. (c) Simulation with initial substrate consisting of bedrock. (d) Bedrock simulation with flexural isostatic uplift in response to the erosional unloading. Effective elastic thickness is 15 km, with a Young's modulus of 100 GPa and Poisson's ratio of 0.25. The dashed line in Figure 8d shows the cumulative amount of isostatic uplift.

contiguous band of high relief. The relative ease with which large valleys can capture drainage on the plateau allows them to grow headward at the expense of their neighbors. Just as in the 1-D experiments, drainage capture and divide migration occur by a combination of differential sediment transport and slope collapse. Capture is made easier by the fact that the slope on the interior plateau is low. The result is that denudation occurs by fluvial dissection rather than by retreat of a coherent escarpment. Thus, even though individual channels may propagate headward over large distances, that by itself is not a guarantee of escarpment retreat.

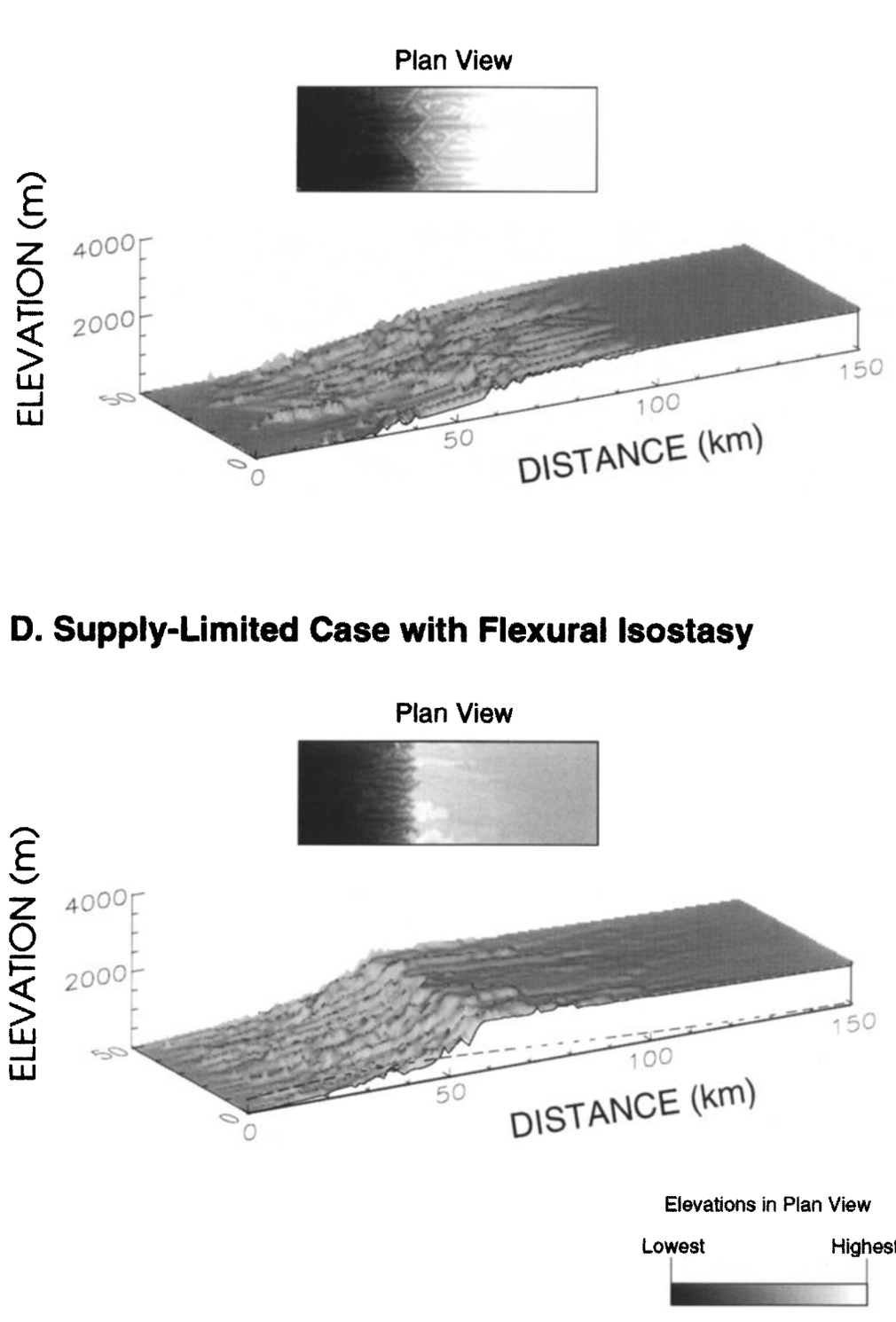

Figure 8. (continued)

Models With Flexural Isostasy

Flexural isostatic uplift in response to denudation is an important process along rifted margins [e.g., *Pazzaglia and Gardner*, this issue]. In the next experiment, we turn on flexure and isostatic adjustment (Figure 8d). Initially, denudation is concentrated along the margin where slopes and relief are greatest. This focused mass removal produces a corresponding isostatic uplift concentrated along the margin. Because the lithosphere has a finite strength (elastic thickness 15 km in this example), the isostatic uplift extends landward so that the effect is to bend the plateau upward along the margin. This tectonic warping accomplishes two things. First, it increases the total relief between the crest of the initial escarpment and base level, thus increasing

stream power and erosion rates. Second, it increases the surface slope on the plateau immediately above the escarpment, thereby making drainage capture by differential sediment transport more difficult. The result is that marginal isostatic uplift makes it harder for the initially larger valleys to gain a competitive advantage by tapping a larger drainage area on the plateau. This process of "equalization" leads to a more uniform pattern of erosional retreat. This physical interpretation is supported by a recent study of the eastern Australian escarpment [*Weissel et al.*, 1992]. The Australian escarpment consists of a series of deeply incised, steep-walled valleys where the drainage divide is far from the escarpment, and a more uniform escarpment face where the drainage divide lies near the escarpment's edge.

The effect of offshore sediment loading depends upon flexural rigidity, as well as upon the distance of the escarpment from the offshore basin. On a rigid lithosphere, offshore sediment loading will create a marginal downwarp that will tend to dampen any erosionally-driven uplift. On the other hand, isostatic uplift of an escarpment will be amplified whenever the flexural bulge from offshore sediment loading comes into phase with the erosionally driven isostatic uplift.

Discussion and Conclusions

The model results presented here suggest that bedrock channel steepening and lateral retreat are viable mechanisms for large-scale, long-term escarpment retreat. Models based on a stream power erosion rule predict that bedrock channels will steepen through time, with a downstream transition to a low-gradient graded reach. This tendency for slope increase is in marked contrast to the behavior of diffusive or transport-limited models, which tend to reduce both slopes and curvature. Thus a supply-limited system characterized by eroding bedrock channels that obey a slope/area-dependent erosion law is a necessary but not sufficient condition for large-scale escarpment retreat in homogeneous material.

For lateral migration of relief to occur, a bedrock channel reach must either be located well downstream of a drainage divide, or it must be capable of driving secondary processes that can move a drainage divide. In the first case, the bedrock channel behaves as a large-scale knickpoint. In the second case, parallel retreat can occur when bedrock channel steepening activates slope failure (or accelerated erosion by other processes, such as debris flows) in its headwaters. In either case, the efficiency of lateral channel retreat in these models depends critically upon two other factors. First, it depends on the balance between sediment supply and sediment transport efficiency. This ratio controls both the length over which a channel approaches its carrying capacity and the slope of the graded reach downstream of the ungraded bedrock portion of the channel. When the sediment supply rate is large relative to transport efficiency, the ungraded, actively incising reach will be shorter, and its tendency to steepen will be impeded. Second, model results suggest that the survival of a bedrock channel eroding the edge of a plateau depends on the elevation of that plateau above base level. Higher relief between the plateau surface and base level allows a channel more freedom to steepen and propagate laterally. Thus high relief is a second necessary (but still not sufficient) condition.

Two-dimensional models that incorporate drainage branching and convergence suggest that when drainage divide migration is rapid relative to the rate of channel steepening and lateral propagation, larger valleys become efficient flow attractors and are thus able to grow at the expense of their neighbors. Where divide migration is impeded, larger drainages lose this competitive advantage and escarpment retreat occurs by more or less uniform advance of a series of closely spaced bedrock channels. This provides a physical mechanism for the observation of *Weissel et al.* [1992] that the morphology of the eastern Australian escarpment varies depending on the location of the drainage divide.

Flexural isostatic uplift provides a mechanism for impeding divide migration and thereby producing a more linear pattern of escarpment retreat. The concentration of denudation along a narrow band produces a focused pattern of isostatic uplift. Thus there is a dynamic coupling between escarpment retreat and isostatic uplift. This coupling will of course be most effective where flexural rigidity is low. The second important effect of isostatic uplift is to increase channel gradients between the top of an escarpment and base level.

The importance of low sediment production rates may seem to imply that Great Escarpments can survive only in arid regions. This is not necessarily the case as witnessed by the bare rock slopes of the Western Ghats escarpment [*Ollier and Powar*, 1985], one of the wettest places on Earth. Any factor that amplifies transport rates over sediment production rates, such as high relief or resistant rocks, can contribute to establishing a supply-limited environment dominated by steep bedrock channels.

Collectively, these model results suggest that the necessary and sufficient conditions for long-term escarpment retreat are (1) incising bedrock channels in which the erosion rate increases with increasing drainage area, (2) a low rate of sediment production relative to sediment transport efficiency, (3) high relief between the top of an escarpment and base level, (4) any process, such as flexural isostatic uplift, that impedes drainage divide migration on the surface above an escarpment.

The above conditions promote relief-generating processes that behave as traveling waves of dissection, rather than diffusive processes which dampen such waves of dissection. Of all the conditions, a high continental elevation above sea level (base level) is common to most escarpment-bounded margins. For example, most of the interior of southern Africa is >1000 m in elevation, and the Deccan Plateau above the Western Ghats is ~800-900 m in elevation. Lower elevation margins, such as the eastern United States, exhibit only smaller, discontinuous escarpments (examples include

the Blue Ridge and Catskill escarpments) that may be remnants of early rift margin escarpments. High continental elevation, which allows for high relief between the interior and coastal base level, may therefore be the most important factor for long-term escarpment survival.

Notation

A drainage area.
C sediment layer thickness.
D flexural rigidity.
x, y horizontal dimensions.
Δx cell width.
E_{BR} average surface lowering rate of a cell containing a bedrock channel segment due to bedrock channel erosion.
E_{MF} surface lowering rate resulting from rock mass failure.
E_W rate of descent of a bedrock/sediment weathering front.
g gravitational acceleration.
h elevation.
k_b proportionality constant for bedrock channel erosion, L^{-1}.
k_d hillslope diffusivity, L^2T^{-1}.
k_f dimensionless sediment transport coefficient.
k_w bare bedrock weathering rate, LT^{-1}.
m_w weathering rate decay constant ($= 1/C_0$, where C_0 is the depth at which the weathering rate reduces to $1/e$ times its surface value, k_w).
l applied crustal load (dimensions of force per unit area).
P effective precipitation rate, LT^{-1}.
Q channel discharge.
q channel discharge per unit width.
q_s fluvial channel sediment flux per unit channel width.
q_{LS}, q_D hillslope sediment flux per unit width due to shallow landsliding and diffusive processes, respectively.
R elevation of the top of a rock column.
S surface slope.
t time.
U tectonic (rock) uplift rate.
w vertical flexural displacement.
ρ_m, ρ_i density of the mantle and of flexural basin infill, respectively.

Acknowledgments. This work was supported by the Earth System Science Center and by a NASA Global Change Fellowship, NGT 30122. We are grateful to M. Gibbs, F. Pazzaglia, and R. Robinson for commenting on early versions of this manuscript and for intellectually fruitful discussion with K. Furlong and T. Gardner. The paper was substantially improved by reviews from A. Gilchrist, H. Kooi, A. Lowry, and D. Merritts.

References

Ahnert, F., Brief description of a comprehensive three-dimensional process-response model of landform development, *Z. Geomorphol. Suppl., 25,* 29-49, 1976.

Anderson, R. S., Evolution of the Santa Cruz Mountains, California, through tectonic growth and geomorphic decay, *J. Geophys. Res.,* this issue.

Anderson, R. S., and N. F. Humphrey, Interaction of weathering and transport processes in the evolution of arid landscapes, in *Quantitative Dynamic Stratigraphy,* edited by T. A. Cross, pp. 349-361, Prentice-Hall, Englewood Cliffs, N. J., 1990.

Bagnold, R. A., An approach to the sediment transport problem from general physics, *U.S. Geol. Surv. Prof. Pap.,* 422-I, 116 pp., 1966.

Beaumont, C., P. Fullsack, and J. Hamilton, Erosional control of active compressional orogens, in *Thrust Tectonics,* edited by K. R. McClay, pp. 1-18, Chapman and Hall, New York, 1992.

Bohannon, R. G., C. W. Naeser, D. L. Schmidt, and R. A. Zimmermann, The timing of uplift, volcanism, and rifting peripheral to the Red Sea: A case for passive rifting?, *J. Geophys. Res., 94,* 1683-1701, 1989.

Bremner, J. M., J. Rogers, and G. F. Birch, Surficial sediments of the continental margin of South West Africa/Namibia, report, Geol. Surv. of South West Africa/Namibia, Windhoek, Namibia, 1988.

Brown, R. W., D. J. Rust, M. A. Summerfield, A. J. W. Gleadow, and M. C. J. De Wit, An early Cretaceous phase of accelerated erosion on the south-western margin of Africa: Evidence from apatite fission track analysis and the offshore sedimentary record, *Nucl. Tracks Radiat. Meas., 17,* 339-350, 1990.

Carson, M. A., and M. J. Kirkby, *Hillslope Form and Process,* 475 pp., Cambridge University Press, New York, 1972.

Chase, C. G., Fluvial landsculpting and the fractal dimension of topography, *Geomorphology, 5,* 39-57, 1992.

Davis, W. M., The geographical cycle, *Geogr. J., 14,* 481-504, 1899.

Flemings, P. B., and T. E. Jordan, A synthetic stratigraphic model of foreland basin development, *J. Geophys. Res., 94,* 3851-3866, 1989.

Gardner, T. W., Experimental study of knickpoint and longitudinal profile evolution in cohesive, homogeneous material, *Geol. Soc. Am. Bull., 94,* 664-672, 1983.

Gerrard, I., and G. C. Smith, Post-Paleozoic succession and structure of the southwestern African continental margin, in *Studies in Continental Margin Geology,* edited by J. S. Watkins and C. L. Drake, AAPG Mem., 34, 49-74, 1982.

Gilbert, G. K., Report on the geology of the Henry Mountains, 160 pp., U.S. Geogr. and Geol. Surv. of the Rocky Mt. Region, Gov. Print. Off., Washington, D. C., 1877.

Gilchrist, A. R., and M. A. Summerfield, Differential denudation and flexural isostasy in the formation of rifted-margin upwarps, *Nature, 346,* 739-742, 1990.

Hoffman, P. F., and J. P. Grotzinger, Orographic precipitation, erosional unloading, and tectonic style, *Geology, 21,* 195-198, 1993.

Howard, A. D., Thresholds in river regimes, in *Thresholds in Geomorphology,* edited by D. R. Coates and J. D. Vitek, Allen and Unwin, Boston, Mass., 1980.

Howard, A. D., Modelling fluvial systems: Rock-, gravel- and sand-bed channels, in *River Channels,* edited by K. Richards, pp. 69-94, Basil Blackwell, New York, 1987.

Howard, A. D., and G. Kerby, Channel changes in badlands, *Geol. Soc. Am. Bull., 94,* 739-752, 1983.

Howard, A. D., M. A. Seidl, and W. E. Dietrich, Modeling fluvial erosion on regional or continental scales (extended abstract), in *AGU Chapman Conference on Tectonics and Topography*, p. 21, AGU, Washington, D.C., 1992.

Howard, A. D., W. E. Dietrich, and M. A. Seidl, Modeling fluvial erosion on regional to continental scales, *J. Geophys. Res.*, this issue.

Iida, T., and K. Okunishi, Development of hillslopes due to landslides, *Z. Geomorphol. Suppl., 46*, 67-77, 1983.

King, L. C., Canons of landscape evolution, *Geol. Soc. Am. Bull., 64*, 721-752, 1953.

King, L. C., Pediplanation and isostasy: An example from South Africa, *Q. J. Geol. Soc. London, 111*, 353-359, 1955.

Kooi, H., and C. Beaumont, Escarpment evolution on high-elevation rifted margins: Insights derived from a surface processes model that combines diffusion, advection and reaction, *J. Geophys. Res.*, this issue.

Koons, P. O., The topographic evolution of collisional mountain belts: A numerical look at the Southern Alps, New Zealand, *Am. J. Sci., 289*, 1041-1069, 1989.

Leopold, L. B., M. G. Wolman, and J. P. Miller, *Fluvial Processes in Geomorphology*, 522 pp., W. H. Freeman, New York, 1964.

Moore, M. E., A. J. W. Gleadow, and J. F. Lovering, Thermal evolution of rifted continental margins: New evidence from fission tracks in basement apatites from southeastern Australia, *Earth Planet. Sci. Lett., 78*, 255-270, 1986.

Moretti, I. and D. L. Turcotte, A model for erosion, sedimentation, and flexure with application to New Caledonia, *J. Geodyn., 3*, 155-168, 1985.

Ollier, C. D., Morphotectonics of continental margins with great escarpments, in *Tectonic Geomorphology*, edited by M. Morisawa and J. T. Hack, pp. 3-25, Allen and Unwin, Boston, Mass., 1985.

Ollier, C. D., and M. E. Marker, The Great Escarpment of southern Africa, *Z. Geomorphol. Suppl., 54*, 37-56, 1985.

Ollier, C. D. and K. B. Powar, The Western Ghats and the morphotectonics of peninsular India, *Z. Geomorphol. Suppl., 54*, 57-69, 1985.

Partridge, T. C., and R. R. Maud, Geomorphic evolution of south- ern Africa since the Mesozoic, *S. Afr. J. Geol., 90*, 179-208, 1987.

Pazzaglia, F. J., and T. W. Gardner, Late Cenozoic flexural defor- mation of the middle U.S. Atlantic passive margin, *J. Geophys. Res.*, this issue.

Penck, W., *Morphological Analysis of Land Forms: A Contribution to Physical Geography*, 429 pp., translated by H. Czech and K. C. Boswell, Macmillan, London, 1953.

Seidl, M. A., and W. E. Dietrich, The problem of channel erosion into bedrock, *Catena Suppl., 23*, 101-124, 1992.

Snow, R. S., and R. L. Slingerland, Mathematical modeling of graded river profiles, *J. Geol., 95*, 15-33, 1987.

Strahler, A. N., *Modern Physical Geography*, 502 pp., John Wiley, New York, 1978.

Stuwe, K., Flexural constraints on the denudation of asymmetric mountain belts, *J. Geophys. Res., 96*, 10,401-10,408, 1991.

Summerfield, M. A., *Global Geomorphology: An Introduction to the Study of Landforms*, 537 pp., Longman Scientific and Technical, London, 1991.

ten Brink, U., and T. Stern, Rift flank uplifts and hinterland basins: Comparison of the Transantarctic Mountains with the Great Escarpment of southern Africa, *J. Geophys. Res., 97*, 569-585, 1992.

Turcotte, D. L., and G. Schubert, *Geodynamics: Application of Continuum Physics to Geological Problems*, 450 pp., John Wiley, New York, 1982.

Weissel, J. K., Long-term erosional development of rifted conti- nental margins: Toward a quantitative understanding, in *Pacific Rim Congress 90* [proceedings], pp. 63-70, Australian Institute of Mining and Metallurgy, Parkville, Victoria, 1990.

Weissel, J. K., and G. D. Karner, Flexural uplift of rift flanks due to mechanical unloading of the lithosphere during extension, *J. Geophys. Res., 94*, 13,919-13,950, 1989.

Weissel, J. K., G. D. Karner, A. Malinverno, and D. J. Harding, Tectonics and erosion: Topographic evolution of rift flanks and rifted continental margins, in *AGU Chapman Conference on Tectonics and Topography*, p. 31, AGU, Washington, D.C., 1992.

Willgoose, G., R. L. Bras, and I. Rodriguez-Iturbe, Results from a new model of river basin evolution, *Earth Surf. Processes Landforms, 16*, 237-254, 1991.

Wolman, M. G., and J. P. Miller, Magnitude and frequency of forces in geomorphic processes, *J. Geol., 68*, 54-74, 1960.

Yalin, M. S., *Mechanics of Sediment Transport*, 2nd ed., 298 pp., Pergamon, New York, 1977.

R. L. Slingerland and G. E. Tucker, Earth Science Center and Department of Geological Sciences, Pennsylvania State University, University Park, PA 16802.

(Received April 2, 1993; revised January 27, 1994; accepted January 31, 1994.)